Dynamics of exciton formation for near band-gap excitations

K. Siantidis, V. M. Axt, and T. Kuhn
Institut für Festkörpertheorie, Westfälische Wilhelms Universität Münster, Wilhelm-Klemm-Strasse 10, D-48149 Münster, Germany
(Received 19 April 2001; revised manuscript received 5 July 2001; published 13 December 2001)

We present a microscopic density matrix description of the formation of excitons after optical excitation of a semiconductor. Three types of dynamical processes taking place after the optical excitation are analyzed: (a) decoherence, (b) incoherent redistributions of occupations among excitonic states or among unbound electron-hole pairs, and (c) formation of excitons. The competition of different scattering mechanisms under varying excitation energies in the vicinity of the band gap is studied for a two band GaAs quantum-wire model. The respective influences of piezoelectric and deformation potential coupling to acoustic phonons, Fröhlich coupling to optical phonons, interface roughness, and radiative decay are compared. A comprehensive picture of the formation process is obtained by following the time evolution of the 1*s* exciton population in dependence of the center of mass momentum. For the times studied here (up to 50 ps) we find no significant impact of radiative decay. All other scattering mechanisms have noticeable influences on the dynamics. Piezoelectric coupling is particularly important for the decoherence above the band gap, while emission of longitudinal optical phonons turns out to be the most efficient process for exciton formation as soon as it is energetically allowed. Exciting at the threshold for the emission of longitudinal optical phonons we find an exciton formation time of ≈ 4 ps at a temperture of 80 K, which increases dramatically when the excitation energy is lowered towards the band edge. The relative importance of the competing mechanisms varies significantly for the different aspects of the dynamics (decoherence, redistribution, formation) and it also depends crucially on the excitation energy. The effects of the different scattering mechanisms are in general not additive.

DOI: 10.1103/PhysRevB.65.035303 PACS number(s): 78.67.Lt, 71.35.Gg, 42.65.Sf

I. INTRODUCTION

It has been widely noticed that after optical excitation of semiconductors above the band gap the relaxation of correlated electron hole pairs and in particular the formation of excitons may have a significant impact on many experiments.[1–15] Thus, e.g., the rise time of the excitonic luminescence after ultrafast excitation at high energies in the band exhibits an oscillatory behavior that has been shown to reflect changes in the efficiency of exciton formation.[6,16] Further evidence for the importance of exciton formation has been found by measuring the spatial expansion rate in time and space resolved pump and probe experiments. Here, for near band-gap excitation an *overshoot* of the rates is observed, which has been interpreted as an indication for the formation of excitons with high kinetic energies of their center-of-mass (c.m.) motion.[11,17]

Recently, experimental studies of the exciton formation and relaxation dynamics have also been performed on quantum-wire systems.[13] From measurements of the time-resolved photoluminescence from a GaAs/AlAs quantum-wire array an exciton formation time of ≈ 30 ps has been extracted.[13] The investigations in Ref. 13 also suggest that exciton-acoustic-phonon scattering is enhanced in an one dimensional system, while exciton-carrier scattering is suppressed.

Calculations related to exciton formation are mostly based on a three particle picture where electrons, holes, and excitons are treated as distinct types of particles.[4,14,16,18–24] In the simplest case one deals with phenomenological rate equations for the corresponding total particle densities.[4] More refined implementations of this idea make use of a set of coupled semiclassical Boltzmann equations for the *k*-space occupations of electrons, holes, and excitons.[14,16,18–24] However, the case of near band-gap excitations considered in the present paper requires a more advanced modeling for several reasons. (i) Electron-hole pairs with energies slightly above the band gap are not well represented by plane waves, which is usually assumed in the three particle picture; instead, noticeable Coulomb induced correlations between electrons and holes have to be expected. (ii) Since any exciton density necessarily contributes to the electron and the hole density there is no strict distinction between the three particle types; although this problem occurs quite generally, it is less severe for excitations far above the band gap, because electron and hole densities related to an exciton are restricted to a *k*-space region up to a few reciprocal Bohr radii and thus there is no noticeable overlap with high energetic particles. (iii) Within the Boltzmann description the laser induced generation of the carriers is accounted for by a corresponding rate. However, closer inspection of the generation process reveals that the laser field is primarily coupled to interband coherences. Thus, in a first step only coherent electron-hole amplitudes are excited. For spatially homogeneous excitations the resulting coherent electron-hole pairs have no center of mass motion. Only after a second step involving scattering events with finite momentum transfer incoherent pair occupations with finite c.m. motion are obtained. Consequently, a microscopic description of the optical generation has to account for coherences in addition to the occupation densities known from the Boltzmann theory. (iv) For excitations several longitudinal optical LO phonon energies above the band gap and low excitation densities polar-optical scattering is usually assumed to dominate the exciton formation process[16,25] while near the band gap there is a variety of competing scat-

tering processes which have to be taken into account simultaneously.

There have been a few recent studies of the conversion dynamics from coherent excitations into incoherent occupations including the corresponding build-up of c.m. kinetic energy using quantum well models.[17,26,27] These studies have all concentrated on excitations in resonance with the 1*s* exciton accounting exclusively for occupations on the 1*s* parabola. Here, we extend these investigations by considering all pair states in the vicinity of the band edge. Thus in addition to the 1*s* parabola we account for higher excited bound excitons as well as for pairs in scattering states. This extension is, of course, indispensable for studies of the redistribution and exciton formation dynamics subsequent to laser excitations above the band gap. But also for resonant excitation at the 1*s* exciton it gives new insights, because we are able to analyze the dynamics of dissociation processes, which is the inverse process to exciton formation. Some authors speak of *exciton formation* when they refer to the conversion from coherent into incoherent pairs subsequent to a selective excitation in resonance with the 1*s* exciton,[27] although in this case the pairs are generated in states on the 1*s* parabola from the start instead of being formed from quasifree electron-hole pairs. We shall follow here the more commonly used convention and denote as *exciton formation* processes where an initially unbound electron-hole pair or a pair in a highly excited state is converted into a density on the 1*s* parabola.

In the present paper we introduce a theoretical framework that describes the dynamics of exciton formation for near band-gap excitation and low excitation densities taking into account the coherent generation process and the Coulomb correlation of electron-hole pairs. Coherent and incoherent electron-hole pairs are treated on the same microscopic level allowing for a consistent modeling of their combined dynamics which is needed to describe the conversion of coherent excitations into incoherent pair occupations. We account for scattering with longitudinal acoustical (LA) phonons via the deformation potential (DP) and piezoelectric (PE) coupling to LA and to transverse acoustical (TA) phonons, interactions with LO phonons via the Fröhlich coupling, scattering due to interface roughness (IR) as well as for radiative decay (RD).

Our goal is to study in detail the dynamics of exciton formation starting with the coherent generation followed by the conversion into incoherent densities and the subsequent incoherent relaxation dynamics. The competition between different scattering mechanisms is analyzed for varying central frequencies of the laser pulse in the vicinity of the band gap.

The paper is organized as follows. In Sec. II we give a brief outline of the theory, introducing the relevant dynamical variables and their equations of motion. Furthermore it is described how the various scattering mechansisms are incorporated into the theory. In Sec. III the numerical results are presented and discussed and finally in Sec. IV we draw conclusions from our results.

II. MICROSCOPIC THEORY

We use a microscopical density matrix description of a two-band quantum wire with a parabolic band structure. Within a microscopic formulation the relevant quasiparticles are electrons and holes described by Fermi operators and phonons represented by Bose operators. Starting from the respective standard Hamiltonians we account for the interactions between these quasiparticles namely the Coulomb interactions between charged carriers[28–30] and the phonon-carrier interactions[31–33] as well as the interaction of electrons and holes with a stochastic interface roughness potential.[34–36] The system is driven by an external laser field which is treated classically and in addition the system is coupled to a quantized light field in order to model the radiative decay.[27,37–40] With exception of the classical laser field all of the above interactions lead to an infinite hierarchy of corresponding higher order density matrices. Thus, the Coulomb interaction results in a hierarchy of electronic density matrices,[28,32,41–44] the phonon coupling gives rise to a hierarchy of phonon assisted density matrices,[32,45–47] while the quantized light field is a source for a hierarchy of photon assisted density matrices.[27,39,40,48] Finally, the interface roughness builds up a hierarchy of correlation functions of the stochastic potential.[35,36] In order to truncate the electronic hierarchy we use the dynamics controlled truncation (DCT) scheme.[28] While DCT was originally formulated for a pure electronic system[28] it has been shown that this concept can be extended to a system also interacting with phonons.[41,47] However, the full DCT treatment including phonons would require the evaluation of high-dimensional generating functions for phonon assisted density matrices and is not practical for a system with a macroscopic number of relevant phonon modes. Therefore, in Ref. 41 a reduced treatment of the phonon branch of the hierarchy has been developed that can be combined with the DCT truncation of the electronic branch. This scheme involves a correlation expansion for phonon asssisted variables in combination with the *Markov* approximation. In the present paper we adopt this strategy for the phonon interaction and apply analogous procedures to all other scattering mechanisms. In the following sections we discuss the resulting selection of dynamical variables and their respective equations of motion and for each scattering mechanism our specific implementation is explained.

A. Dynamical variables

We are interested in the low density regime where it is sufficient to keep only contributions up to second order in the laser field. For low excitation densities there are two types of electronic variables that are revelant for the discussion of exciton formation:[26,41] the interband transition amplitude

$$Y_2^1 := \langle \hat{Y}_2^1 \rangle := \langle d_1 c_2 \rangle, \tag{1}$$

and the correlated part of the electron-hole pair density

$$\overline{N}_{1\,4}^{2\,3} := \langle \hat{Y}_1^{2\dagger} \hat{Y}_4^3 \rangle - Y_1^{2*} Y_4^3, \tag{2}$$

where c_j (d_j) are Fermi operators annihilating electrons (holes) in Wannier states located at sites $\mathbf{r}_j$ with spin σ_j. It should be noted that it is not necessary to consider the densities $\langle c_1^\dagger c_2 \rangle$ and $\langle d_1^\dagger d_2 \rangle$ of electrons and holes as dynamical

variables in their own right, because these quantities can be eliminated in favor of Y and $\overline{N}$ by using identities that are exact within a second order treatment.[41,47,49] Furthermore, due to the use of the Markov approximation also all assisted variables are eliminated and thus do not show up explicitely as dynamical variables in the equations of motion of Y and $\overline{N}$. Their influence is approximately taken into account via corresponding self-energies. The pair amplitude Y contains the information about coherent electron-hole pairs that are either bound (excitons) or in scattering states. Since the interband polarization is directly related to the interband transition amplitude Y, the latter determines coherently emitted optical signals such as linear transmission, four-wave mixing or pump and probe signals. $\overline{N}$ describes incoherent occupations of bound and unbound electron-hole pair states as well as intraband coherences. The latter are, e.g., the driving sources for the THz emission.[50,51] The pair occupations, in contrast, are direct sources for secondary emission such as luminescence signals.[16,27,39,40] While standard luminescence monitors pair occupations with nearly vanishing ($K\approx 0$) c.m. momentum,[16] it has been demonstrated that it is possible to measure the exciton occupation density as a function of K over a broad K region by using LO phonon-assisted photoluminescence. Corresponding measurements have been performed in bulk Cu_2O (Refs. 52,53) as well as in ZnSe quantum wells.[25,54]

B. Equations of motion

We performed all calculations in the electron-hole pair basis. The transformation between the real space representations Y and $\overline{N}$ of the relevant dynamical variables and their counterparts y and $\overline{n}$ in pair reprensentation is given by

$$Y_2^1=\sum_x \Psi_{12}^x y_x, \tag{3}$$

$$\overline{N}_{1\,4}^{2\,3}=\sum_{xx} \Psi_{21}^{\overline{x}*}\Psi_{34}^x \overline{n}_{\overline{x}x}, \tag{4}$$

where Ψ^x is the wave function of an electron-hole pair in the state x corresponding either to a bound exciton state or to an electron-hole scattering state. In this paper we treat a quantum-wire model with infinitely high barriers and concentrate exclusively on the lowest sublevel. Thus we deal effectively with an one dimensional problem where the motion of the electron-hole pairs is restricted to a motion along the wire axis. It is well known that for a quasi-one-dimensional system it is important to account for the finite extension in the confined directions. Thus we have considered a cylindrical wire of finite width. In this case the multiindex $x=(K,\nu)$ stands for the center of mass momentum K and the quantum number ν of the relative motion of the pairs and thus the pair wave-function Ψ_{12}^x reads

$$\Psi_{12}^x := \Psi_{12}^{K,\nu} := \frac{e^{iKR_{12}}}{\sqrt{L}}\varphi_\nu(r_{12})u_{\rm h}(r_{1\perp})u_{\rm e}(r_{2\perp}). \tag{5}$$

Here, L is a normalization length, R_{12} and r_{12} are, respectively, the c.m. and the relative real space coordinates in wire direction, while $r_{2\perp}$ and $r_{1\perp}$ are the coordinates of the electron and the hole perpendicular to the wire. $\varphi_\nu(r_{12})$ is the wave function for the relative motion of the pair in state ν and $u_{\rm e/h}(r_\perp)$ are the confinement functions for electrons/holes corresponding to the lowest wire sublevel.

Applying the DCT scheme combined with the Markov approximation for the scattering processes as discussed above we obtain the following equations of motion:

$$i\hbar\partial_t y_x=\hbar\omega_x y_x-\mathbf{E}\mathbf{M}_x+\sum_{x'}\hbar\Omega_{Y_x}^{\ x'}y_{x'}+i\hbar\partial_t y_x|_{\rm RD}, \tag{6}$$

$$\begin{aligned} i\hbar\partial_t \overline{n}_{\overline{x}x}=\hbar(\omega_x-\omega_{\overline{x}})\overline{n}_{\overline{x}x}-\sum_x [y_{\overline{x}}^*(\hbar\Omega_{Y_x}^{\ x'}y_{x'}) \\ -y_x(\hbar\Omega_{Y_{\overline{x}}}^{\ \overline{x}}y_{x'})^*]+\sum_{x'x'}\hbar\Omega_{N_{\overline{x}\,x}^{\overline{x}'\,x'}}(\overline{n}_{\overline{x}'x'}+y_{\overline{x}'}^*y_{x'}) \\ +i\hbar\partial_t\overline{n}_{\overline{x}x}|_{\rm RD}, \end{aligned} \tag{7}$$

where $\hbar\omega_x$ is the energy for an interband transition to the pair state x, $\mathbf{M}_x$ is the dipol-matrix element in the pair representation, and $\mathbf{E}$ is the external laser field. $\partial_t y_x|_{\rm RD}$ and $\partial_t\overline{n}_{\overline{x}x}|_{\rm RD}$ account for the radiative decay which is the only scattering process that does not conserve the total number of electron-hole pairs. All other scattering processes enter via self-energy matrices $\hbar\Omega$ of the form

$$\hbar\Omega_{Y_x}^{\ x'}=\sum_{\tilde{x}}\Gamma_{x\tilde{x}\overline{\tilde{x}}x'}, \tag{8}$$

$$\begin{aligned} \hbar\Omega_{N_{\overline{x}x}}^{\overline{x}'x'}=\delta_{\overline{x}x'}\sum_{\tilde{x}}\Gamma_{x\tilde{x}\tilde{x}x'}-\delta_{xx'}\sum_{\tilde{x}}\Gamma_{\tilde{x}\tilde{x}\overline{\tilde{x}}x'}^*+\Gamma_{x'x\overline{x}x'}^* \\ -\Gamma_{\overline{x}'\overline{x}xx'}, \end{aligned} \tag{9}$$

where each scattering mechanism adds a specific contribution to $\Gamma_{xx'\overline{xx'}}$. $\partial_t y_x|_{\rm RD}$ and $\partial_t\overline{n}_{\overline{x}x}|_{\rm RD}$ are detailed below as well as the coupling matrices $\Gamma_{xx'\overline{xx'}}$ for each scattering mechanism. It should be noted that the Markov approximation depends crucially on the basis and therefore a choice is needed that is well adapted to the physics under consideration. In the Appendix we discuss in detail the physical implications of the Markov approximation in particular with respect to a proper description of exciton formation processes and explain why the electron-hole pair basis is a suitable choice in our case.

Equation (6) describes the generation of coherent electron-hole pairs and their decay. Note that y_x is the coherent amplitude which is related to the corresponding pair density $N_{\rm coh}^x$ by $N_{\rm coh}^x=|y_x|^2$ and thus the total coherent pair density $N_{\rm coh}$ is given by

$$N_{\rm coh}=\sum_x |y_x|^2. \tag{10}$$

The first term in Eq. (6) represents the free oscillation of the interband transition with frequency ω_x that is driven by the external laser field in the second term. The third term is responsible for the dephasing due to phonons and interface roughness while the last term accounts for the radiative decay. The off-diagonal elements of $\overline{n_{xx}}$ describe coherences between different pair states while the diagonal elements stand for the incoherent pair occupations. Thus the total incoherent pair density N_{incoh} is given by

$$N_{\mathrm{incoh}}=\sum_x \overline{n_{xx}}. \tag{11}$$

By choosing y and $\overline{n}$ as dynamical variables a natural separation between coherent and incoherent densities without overlap is achieved, such that the total pair density N_{tot} is simply the sum of the two components

$$N_{\mathrm{tot}}=N_{\mathrm{coh}}+N_{\mathrm{incoh}}. \tag{12}$$

As in the y equation, the first term on the right hand side of Eq. (7) is responsible for a free oscillation. The second term acts as a source for $\overline{n_{xx}}$ and describes the transformation of coherent excitations into incoherent pair densities. The third term results from the interaction with phonons and interface roughness. Due to the form (9) of the self-energy matrices $\hbar\Omega_N$ it is easy to see that $\Sigma_x \hbar\Omega_{N\,x}^{\overline{x'}\,x'}=0$. Therefore, this term does not change the total number of incoherent pairs N_{incoh} as expected for interactions that provide only couplings either within the conduction or within the valence band. Consequently, $\hbar\Omega_N$ leads to a redistribution of the pair densities. Furthermore, from Eqs. (6) and (7) it follows immediately that the total number of pairs N_{tot} is only changed either by the laser field coupling, which drives the pair generation, or by radiative decay. Of course, this reflects the fact that the laser induced generation and the radiative decay are the only processes in our model that provide for interband couplings. However, it also follows from this consideration that the second term on the right-hand side of Eq. (7) is indeed a source for incoherent densities that equals the loss of the corresponding coherent densities induced by the intraband scatterings proportional to $\hbar\Omega_Y$, in accordance with our interpretation that this term represents the conversion of coherent excitations into incoherent occupations. It should be noted that although in this paper we present numerical results for an effectively one dimensional system the form of Eqs. (6)–(12) applies also for higher dimensional systems such as quantum wells or bulk materials.

C. Phonon scattering

We account for carrier-phonon interactions with acoustical and optical phonons. In both cases the phonon modes will be identified with the modes of a three dimensional system assuming that the wire and the barrier material do not differ significantly in their lattice and dielectric properties. For a band gap that is of the order of optical frequencies phonon scattering can be considered as a pure intraband process. Thus, application of the Markov approximation yields contributions to the self-energies $\hbar\Omega_Y$ and $\hbar\Omega_N$ that are governed by corresponding coupling matrices $\Gamma_{xx'\overline{xx'}}$ [see Eqs. (8) and (9)]. The contribution $\Gamma^{\mathrm{ph}}_{xx'\overline{xx'}}$ resulting from the carrier-phonon interaction has been derived in Ref. 41 and has the following form:

$$\Gamma^{\mathrm{ph}}_{xx'\overline{xx'}}=\sum_\mu \frac{-i\pi}{\hbar}[\Gamma^{\mu}_{xx'}\Gamma^{\mu *}_{\overline{x'}\overline{x}} n_\mu \delta(\omega_{\overline{x'}}-\omega_{\overline{x}}+\omega_\mu) + \Gamma^{\mu *}_{x'x}\Gamma^{\mu}_{\overline{xx'}}(n_\mu+1)\delta(\omega_{\overline{x'}}-\omega_{\overline{x}}-\omega_\mu)], \tag{13}$$

where $\Gamma^{\mu}_{xx'}$ are matrix elements in the electron-hole pair basis describing the coupling to the phonon mode μ with frequency ω_μ and n_μ is the corresponding thermal occupation $n_\mu=1/[\exp(\hbar\omega_\mu/k_BT)-1]$. A phonon mode μ is characterized by specifying the corresponding three-dimensional wave vector $\mathbf{q}$ and the phonon branch j which can be either acoustic or optical. Therefore, the sum in (13) involves a summation over the branches as well as over $\mathbf{q}$.

By projecting the standard three dimensional phonon coupling[32,33,46] onto the lowest wire sublevel and denoting the Fourier transform of $\varphi_\nu(r_{12})$ by $\varphi_\nu(k)$ one obtains explicitely for the phonon coupling in the pair basis

$$\Gamma^{\mu}_{xx'}:=\Gamma^{j,\mathbf{q}}_{\nu\nu'}(K,K'):=\frac{\delta_{q_\parallel,K'-K}}{2\pi\sqrt{L}} f(q_\perp)\int_{-\infty}^{\infty} dk\,\varphi^*_\nu(k) \times[\gamma^e_\mu \varphi_{\nu'}(k-\mu_h q_\parallel)-\gamma^{\mathrm{h}}_\mu \varphi_{\nu'}(k+\mu_e q_\parallel)]. \tag{14}$$

Here, $q_\parallel$ and $q_\perp$ are, respectively, the phonon wave-vector components in the wire direction and perpendicular to it and $\mu_{e/h}:=m_{e/h}/(m_e+m_h)$ are the fractions of the electron/hole masses $m_{e/h}$ with respect to the total mass m_e+m_h. The masses $m_{e/h}$ refer to the motion in wire direction. $\gamma^{e/h}_\mu$ is the coupling of an electron/hole to the phonon mode μ of the three-dimensional system. The form factor $f(q_\perp)$ stems from the projection onto the lowest subband of the wire and is defined as

$$f(q_\perp):=\sum_{r_\perp} u_{\mathrm{h}}(r_\perp)u_{\mathrm{e}}(r_\perp)e^{iq_\perp r_\perp}. \tag{15}$$

The representation (14) is valid for the interaction with both acoustical and optical phonons as well as for different carrier-phonon coupling mechanisms, which are distinguished only by different $\mathbf{q}$ dependencies of the functions $\gamma^{e/h}_\mu$ that may be specified for each of the mechanisms discussed in this paper as follows.

1. Acoustic phonon scattering

Acoustical phonons are coupled to the carriers via the deformation potential as well as via the piezoelectric coupling. While the deformation potential exclusively couples to LA phonons, the piezoelectric scattering with both LA and TA phonons is appreciable; usually the piezoelectric scattering with TA phonons is significantly stronger than with LA phonons due to the smaller sound velocity.[55] Accounting to-

gether for piezoelectric and deformation potential interactions the coupling $\gamma_{\mathrm{AC}}^{e/h}$ to acoustic phonons can be represented as[33,55]

$$\gamma_{\mathrm{AC},j,\mathbf{q}}^{e/h}=\sqrt{\frac{\hbar}{2\varrho\,\omega_j(q)}}(q\,D_j^{e/h}+iM_j(\hat{q})), \tag{16}$$

where $q:=\sqrt{q_\parallel^2+q_\perp^2}$ is the modulus of $\mathbf{q}$ and $\hat{q}$ is the unit vector in the direction of $\mathbf{q}$. $\omega_j(q)$ represents the dispersion for the acoustical phonons, ϱ is the density of the semiconductor, $D_j^{e/h}$ stands for the deformation potential constants for electrons or holes, and M_j provides for the piezoelectric coupling. The branch index j runs over the longitudinal and the two transverse modes and the constants $D_j^{e/h}$ are nonvanishing only for the LA mode. As only phonons near the center of the Brillouin zone are efficiently coupled to the electron-hole pairs it is justified to assume a linear dispersion $\omega_j(q)=v_j q$, where v_j is the sound velocity in the material that, depending on the mode, has to be identified with either the velocity of longitudinal or shear waves. It should be noted that although it is the square module of $\gamma_{\mathrm{AC},\mathbf{q}}^{e/h}$ that finally enters the dynamics via Eq. (13), there is no mixing between deformation potential and piezoelectric scattering, because the former gives a real and the latter provides for a purely imaginary contribution to Eq. (16). As discussed in Refs. 33,55, the piezoelectric coupling would in principle introduce an anisotropy that is, however, usually ignored. Instead, an effective isotropic model is considered that may be obtained by averaging over the angles. More specifically, because it is the square of $M(\hat{q})$ that introduces the anisotropy in Eq. (13) an angle average over this quantity is needed. For a crystal with zinc-blende structure the averaging yields[55]

$$\frac{1}{4\pi}\int_0^{2\pi}d\varphi\int_0^{\pi}d\theta\sin(\theta)M_j^2(\hat{q})=A_j\left(\frac{2\,e\,e_{14}}{\varepsilon_s\varepsilon_0}\right)^2, \tag{17}$$

where e_{14} is the piezoelectric coeficient, ε_0 stands for the vacuum susceptibility, e denotes the elementary charge, ε_s is the static dielectric constant, and A_j are mode dependent geometrical factors that can be found, e.g., in Ref. 55.

2. Optical phonon scattering

We treat LO phonons as dispersionless quasiparticles with a constant frequency ω_{LO}. LO phonons interact with the carriers dominantly via the polar-optical Fröhlich coupling which has the well known form

$$\gamma_{\mathrm{LO},q}^{e/h}=\gamma_{\mathrm{LO},q}=i4\pi\sqrt{\frac{e^2\hbar}{2\,\alpha\,\omega_{\mathrm{LO}}}}\frac{1}{q}, \tag{18}$$

with

$$\alpha^{-1}=\frac{\omega_{\mathrm{LO}}^2}{\varepsilon_0\,(4\pi)^2}\left(\frac{1}{\varepsilon_\infty}-\frac{1}{\varepsilon_s}\right),$$

where ε_∞ is the high frequency dielectric constant.

D. Interface roughness scattering

As mentioned above also the dynamical impact of interface roughness may be represented as an open hierarchy of correlation functions of the stochastic potential. This approach has been worked out in Refs. 35,56,57. In combination with the Markov approximation the following contribution to the coupling matrices $\Gamma_{xx'\overline{xx'}}$ in Eqs. (8) and (9) is obtained:

$$\Gamma_{xx'\overline{xx'}}^{\mathrm{IR}}=\frac{-i\pi}{\hbar}\langle V^{xx'}V^{\overline{xx'}}\rangle\delta(\omega_{\overline{x}}-\omega_{\overline{x'}}), \tag{19}$$

where $\langle V^{xx'}V^{\overline{xx'}}\rangle$ is the disorder potential correlation function in pair representation.[35,56,57] The case $\overline{x}=\overline{x'}$ has to be excluded because this would correspond to a self-scattering. In this paper we assume a deltalike correlation for the spatial fluctuations of the potential. This assumption yields for the correlation function in pair representation

$$\langle V^{xx'}V^{\overline{xx'}}\rangle=\frac{\hbar}{2\pi}\sigma_{\mathrm{IR}}\sigma_{xx'\overline{xx'}}, \tag{20}$$

where σ_{IR} is a parameter that determines the strength of the interface induced scattering and

$$\sigma_{xx'\overline{xx'}}:=\delta(K'-K+\overline{K'}-\overline{K})\sigma_{\nu\nu'\overline{\nu\nu'}}(K'-K) \tag{21}$$

accounts for the overlap of the pair states involved with

$$\begin{aligned}\sigma_{\nu\nu'\overline{\nu\nu'}}(Q)=&\,\mu_e^2F^{\nu\nu'}(\mu_eQ)F^{\overline{\nu\nu'}}(-\mu_eQ)\\&+\mu_h^2F^{\nu\nu'}(-\mu_hQ)F^{\overline{\nu\nu'}}(\mu_hQ)\\&+\mu_e\mu_h[F^{\nu\nu'}(\mu_eQ)F^{\overline{\nu\nu'}}(\mu_hQ)\\&+F^{\nu\nu'}(-\mu_hQ)F^{\overline{\nu\nu'}}(-\mu_eQ)],\end{aligned} \tag{22}$$

and

$$F^{\overline{\nu\nu}}(\mu Q)=\frac{1}{2\pi}\int_{-\infty}^{\infty}dk\,\varphi_\nu^*(k)\varphi_{\overline{\nu}}(k+\mu Q). \tag{23}$$

It should be noted that in the above treatment in addition to the quantum mechanical averaging an ensemble averaging with respect to different realizations of the interface roughness is implied. Here we are interested in the average effect of interface roughness on the dynamics of pair relaxations. The averaging aspect is also important for discussions of the secondary emission, especially in view of the non-self-averaging character of specle spectroscopy. A further consequence of the double averaging is that it is now possible to discuss different degrees of coherence, because after performing the quantum mechanical average on a single realization there is in general a certain phase coherence with the excitation present that will be reduced in ensemble averaged results. This reduction of phase coherence is reflected by a corresponding contribution to the incoherent pair density $\overline{N}$, which is easily separated from other contributions that result from inelastic scattering processes. This separation is

achieved by making the following decomposition (here we suppress the obvious indices):

$$\bar{N} = \langle \hat{Y}^\dagger \hat{Y} \rangle - \langle \hat{Y}^\dagger \rangle \langle \hat{Y} \rangle$$

$$\overset{\text{cf.(2)}}{=} \underbrace{\langle \hat{Y}^\dagger \hat{Y} \rangle - \langle \langle \hat{Y}^\dagger \rangle_Q \langle \hat{Y} \rangle_Q \rangle_E}_{\textit{inelastic}} + \underbrace{\langle \langle \hat{Y}^\dagger \rangle_Q \langle \hat{Y} \rangle_Q \rangle_E - \langle \hat{Y}^\dagger \rangle \langle \hat{Y} \rangle}_{\textit{elastic}}, \quad (24)$$

where $\langle \cdots \rangle_Q$ denotes the quantum mechanical and $\langle \cdots \rangle_E$ the ensemble average. Throughout this paper we will stick to the convention that an average $\langle \cdots \rangle$ without further specification refers to the double average with respect to quantum mechanics and to the disorder ensemble. Obviously, our definition of $\bar{N}$ implies that we have extracted those coherences from the total pair density that survive both averaging procedures. A separate treatment of elastic and inelastic contributions according to the decomposition (24) has been presented in Refs. 36, 58. However, this distinction is not important for our present discussion and will not be pursued here any further.

E. Radiative decay

To include radiative decay of electron-hole pairs we proceed along the lines as described in Refs. 27,39. In short, we decouple the hierarchy of photon assisted density matrices by invoking the correlation expansion and then eliminate the assisted density matrices by means of the Markov approximation in complete analogy to the treatment of the phonon interaction. In this way the following additional contributions on the right-hand side of Eqs. (6) and (7) are obtained:

$$i\hbar \partial_t y_x|_{\mathrm{RD}} = -i \sum_{x'} D_{\mathrm{RD}}^{xx'x'} y_{x'}, \quad (25)$$

$$i\hbar \partial_t \bar{n}_{xx}|_{\mathrm{RD}} = -i \sum_{x'} [D_{\mathrm{RD}}^{xx'\bar{x}} \bar{n}_{x'\bar{x}} + D_{\mathrm{RD}}^{x'\bar{x}x} \bar{n}_{x'x}], \quad (26)$$

$$D_{\mathrm{RD}}^{xx'\bar{x}} := \sum_q \Delta_q^x \Delta_q^{x'*} \delta(\hbar\omega_{\bar{x}} - E_q), \quad (27)$$

where q and E_q are, respectively, the momentum and energy of the photon and Δ_q^x is the carrier photon coupling matrix element in pair representation. Equation (25) is responsible for the radiative polarization decay while Eq. (26) accounts for the decay of incoherent pair occupations.

III. NUMERICAL RESULTS

We applied our theory to a GaAs quantum-wire with a cylindrical cross section of 100 nm^2. We have used the standard literature values for the material parameters that are listed in Table I. The valence band structure has been modeled using the axial approximation of the Luttinger Hamiltonian such that the heavy hole masses in wire direction and perpendicular to it are connected to the Luttinger parameters by $m_{hh\parallel} := m_h = m_0/(\gamma_1 - 2\gamma_2)$ and $m_{hh\perp} = m_0/(\gamma_1 + \gamma_2)$, respectively, where m_0 is the free electron mass. The pair wave functions $\varphi_\nu(k)$ required for the evaluation of all scattering matrix elements have been determined by a direct diagonalization of the corresponding eigenvalue problem in k space. The convergence of the results with respect to the k space discretization has been carefully tested. All calculations presented here have been performed for a temperature of $T = 80$ K. The temperature dependence of our results will be discussed elsewhere.[59] We have analyzed the dynamics of coherent and incoherent electron-hole pairs after excitation of the system with a Gaussian shaped laser pulse of 250 fs duration corresponding to the full width at half maximum of the intensity. We have taken the pulse maximum as the zero of the time axis. Four different scenarios are considered corresponding to excitations with central frequencies (a) in resonance with the 1s exciton, (b) at the band edge, (c) just below the threshold for transitions to the 1s parabola due to LO phonon emission, (d) slightly above the LO threshold. The pulse spectra for these scenarios are plotted together with the linear absorption spectrum in Fig. 1. The 1s exciton is clearly visible in the linear spectrum while the 2s exciton and higherbound states merge with the band gap. Also plotted is a schematic view of the processes that redistribute the electron-hole pairs after their coherent excitation with vanishing c.m. motion. The scheme illustrates typical pathways for an electron-hole pair scattered by one of the mechanisms discussed in this paper.

TABLE I. Material parameters taken from Ref. 16 except for γ_1, γ_2, v_S, and e_{14} which are taken from Ref. 64 and M_0 from Ref. 27. m_0 is the free electron mass and e the elementary charge.

band-gap energy E_{gap}	1519 meV
effective electron mass m_{e}	0.063 m_0
Luttinger parameter γ_1	6.85
Luttinger parameter γ_2	2.1
LO phonon energy $\hbar\omega_{\mathrm{LO}}$	36.4 meV
static dielectric constant ϵ_s	12.9
high frequency dielectric constant ϵ_∞	10.92
density ρ	5.37 g/cm^3
logitudinal sound velocity v_{L}	5330 m/s
shear sound velocity v_{S}	3343.60 m/s
deformation potential for electrons D^{e}	7000 meV
deformation potential for holes D^{h}	-3500 meV
piezoelectric constant e_{14}	0.16 C/m^2
dipole matrix element M_0	4 e Å

A. Loss of coherence

The excitation with a coherent laser field leads, in a first step, to coherent electron-hole pairs that are described in our formalism by the coherent pair amplitudes y_x. As a result of the scattering processes that set in already during the generation of the pairs, a decay of the coherent amplitudes is initi-

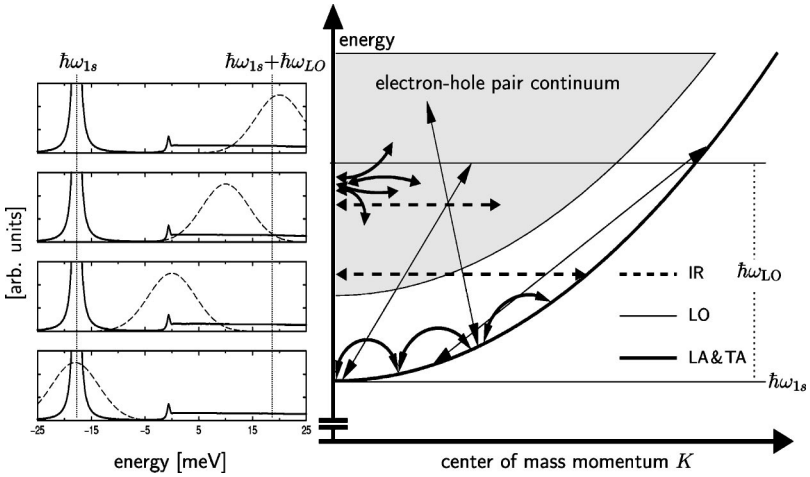

FIG. 1. Left: pulse spectra (dashed line) for the four excitation scenarios discussed in the text in comparison with the calculated linear absorption spectrum (solid line) of our quantum wire. The central frequencies correspond to energies relative to the band edge: −18, 0, 10, 20 meV. Right: schematic view of typical pathways of electron-hole pairs scattered by one of the mechanisms discussed.

ated. The corresponding decay of the coherent pair occupation density N_{coh} defined in Eq. (10) is a direct measure for this loss of coherence. Note, that the decay of the macroscopic polarization

$$P=\sum_x M_x^* \varphi_x(r=0) y_x \tag{28}$$

after short pulse excitation will usually take place on a shorter time scale because superimposed to the decoherence induced by scattering is the dephasing due to destructive interference of the pair oscillators y_x. In order to analyze the influences of the various scattering mechanisms on the decoherence we have determined N_{coh} from a numerical solution of Eq. (6). Figures 2(a)–2(d) correspond to our four excitation scenarios and show for each central frequency separately the contributions of different mechanisms to the decay. In order to facilitate the comparison between the curves with respect to their decay properties we have scaled the resulting densities such that the respective maxima have approximately the same heights.

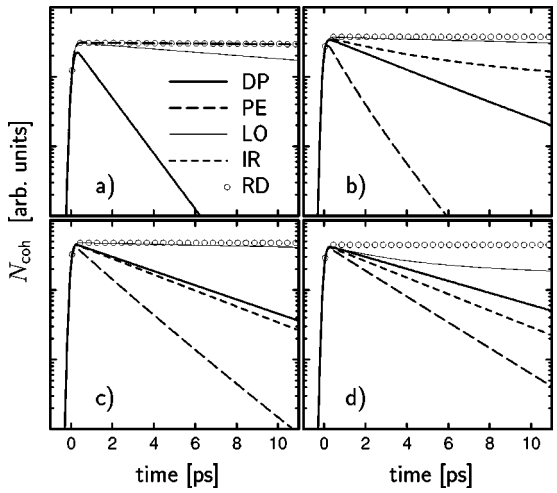

FIG. 2. Time-evolution of N_{coh} for excitation energies relative to the band edge: (a) −18, (b) 0, (c) 10, (d) 20 meV (see Fig. 1). Each curve accounts exclusively for a single scattering mechanism: DP: deformation potential scattering, PE: piezoelectric coupling, LO: Fröhlich coupling, IR: interface roughness scattering with $\sigma_{\mathrm{IR}}=0.02$ meV/ps, RD: radiative decay.

We find a competition of a variety of comparable contributions from different scattering mechanisms. The relative weights of these contributions change significantly with changing excitation conditions. The dependencies reveal that the influence of Coulomb correlations in the vicinity of the band edge is not exausted by the well known modifications of the absorption spectrum (occurrence of the exciton line, Coulomb enhancement), but all scattering mechanisms are strongly affected. Particularly striking is the impact on polar interactions such as the piezoelectric coupling or the Fröhlich interaction, which are significantly reduced when either the initial or the final state is on the 1*s* parabola. This may be easily understood by an intuitive argument, because the exciton is a neutral entity and being a bound state it has a spatially localized wavefunction and therefore contributions from the scattering of an electron and scattering of a hole lead to partial cancelations for polar interactions.[60] As a consequence the loss of coherence due to piezoelectric scattering is negligible for resonant excitation of the 1*s* exciton [see Fig. 2(a)], but it becomes the dominante dephasing mechanism just above the band egde [see Figs. 2(b)–2(d)]. As a general trend piezoelectric scattering decreases with increasing excitation energy for above band edge excitation because the piezoelectric coupling is particularly strong for transitions involving small momentum transfers [see Eq. (16)] and at the band edge there is an increased density of states with small momenta.

The general reduction of polar interactions involving excitons has also an important effect on the Fröhlich coupling. Of course, the small contribution of the LO phonon scattering to the dephasing of the 1*s* exciton [see Fig. 2(a)] is due to the fact that only absorption processes are energetically allowed in this case. The correlation induced reduction of the Fröhlich coupling manifests itself in rather long decay times of the order of several pico seconds [see Fig. 2(d)] just above the threshold for the emission of LO phonons, where the final states of the scattering are on the 1*s* parabola. By calculating the phonon emission rates for a wider energy range we have verified that decay times of the order of ~150 fs,

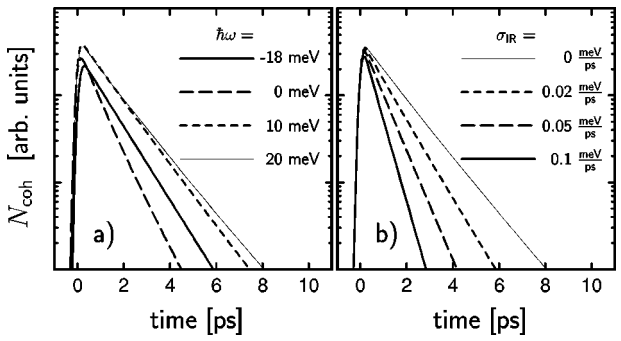

FIG. 3. Time evolution of N_{coh}: (a) calculations for different excitation energies $\hbar\omega$ including all mechanisms except for interface roughness, (b) calculations including all mechanisms for an excitation 20 meV above the band-gap with varying interface roughness strength σ_{IR}.

which are usually associated with the emission of LO phonons, are indeed obtained above the threshold for transitions within the pair continuum.[49] Thus, LO phonon emission dominates only above this second threshold, while reaching the low energetic threshold raises the LO contribution to the dephasing merely to a level comparable with other competing mechanisms. Note that if performing the Markov approximation in the *k*-space basis only this second threshold for LO scattering within the continuum is obtained (see the Appendix) while the low-energetic threshold for LO phonon induced transitions towards the 1*s* parabola is absent. Obviously, the *k*-space version of the Markov approximation misses important aspects of the relaxation dynamics near the band edge.

While polar interactions are reduced due to Coulomb renormalizations almost the reverse tendencies are obtained for deformation potential scattering. For resonant excitation [part (a) of Fig. 2] the loss of coherence is clearly dominated by the deformation potential interaction such that all other mechanisms can be regarded as small corrections. This situation changes when the central frequency is tuned above the band edge, where the contribution from deformation potential coupling decreases. The strength of the deformation potential scattering on the 1*s* parabola is explained by favorable excitonic form factors in Eq. (14). Here, contributions from the scattering of electrons or holes exhibit much weaker compensations than for polar interactions.

Radiative decay turns out to be the only interaction mechanisms which is negligible on the time scale of Fig. 2 for all scenarios studied. While this process is more important in quantum wells[27,38] for wires it evolves on a different time scale. In accordance with previous investigations[37] we find intrinsic radiative decay times for the coherent pair occupations that depend on the pair state but are in any case larger than ~ 150 ps. This effect has been attributed in Refs. 13,37 to a reduced spatial excitonic coherence in one dimensional systems.

Figure 3(a) compares the time evolution of N_{coh} for our four excitation scenarios when all scattering mechanisms except for interface roughness are taken into account. The loss of coherence is fastest when the central frequency is tuned to the band edge. Thus, the increase in efficiency of the piezoelectric coupling compared to the resonant excitation at the 1*s* exciton overcompensates the corresponding reduction of the deformation potential scattering. A further increase of the central frequency above the band gap leads to a slowing down of the decoherence. Changing the central frequency from 10 to 20 meV above the band gap (see Fig. 1) leads to a loss of efficiency of the acoustic phonon scattering processes which even overcompensates the onset of the LO phonon emission.

As an interesting side aspect of our numerical analysis of the time evolution of N_{coh} we have found that the results of calculations where only the diagonal elements of the scattering matrices $\hbar\Omega_{Y_x^{x'}}$ in Eq. (6) are taken into account are not significantly different from the full calculations where also the off-diagonal elements are kept. In order to simplify the numerics we have made use of this diagonal dominance and accounted only for the diagonal elements in the rest of our analysis.

Finally, part (b) of Fig. 3 illustrates the impact of interface roughness on the loss of coherence for an excitation above the LO threshold. The efficiency of interface roughness scattering is decisively determined by the parameter σ_{IR} in Eq. (20) which depends on the quality of the individual sample. Figure 3(b) shows the expected decrease of the decay times with increasing σ_{IR}. The N_{coh} transients resulting only from interface roughness corresponding to a value of $\sigma_{\mathrm{IR}} = 0.02$ meV/ps have been included in the Figs. 2(b)–2(d). Because interface roughness is an elastic scattering process it is only effective above the band edge (see Fig. 1). From the Figs. 2(b)–2(d) it can also be seen that the contribution of interface roughness to the decay increases with increasing excitation energy and for $\sigma_{\mathrm{IR}} = 0.02$ meV/ps it has a magnitude roughly comparable with the effect of the deformation potential. This value of σ_{IR} has been chosen for the subsequent investigations of the influence of interface roughness on the formation of excitons.

B. Conversion into incoherent pair occupations

The loss of coherence is accompanied by a build up of incoherent pair occupations. The most direct measure for quantifying the formation of excitons is the total number $N_{1s} := \Sigma_K \overline{n}_{(1s,K)(1s,K)}$ of pairs occupying states on the 1*s* parabola. It is therefore a natural decomposition to split the total number of pairs into three parts according to

$$N_{\mathrm{tot}} = N_{\mathrm{coh}} + N_{1s} + N_{\mathrm{ex}}, \tag{29}$$

where $N_{\mathrm{ex}} := \Sigma_K \Sigma_{\nu \neq 1s} \overline{n}_{(\nu,K)(\nu,K)}$ measures the total incoherent occupation of excited pair states, i.e., all states not on the 1*s* parabola. In order to obtain the relevant information on the incoherent densities we have solved in addition to Eq. (6) for the amplitudes y_x also Eq. (7) for the incoherent densities using the same excitation conditions as discussed in the previous section. Here, we have concentrated on the dynamics of the occupation densities (diagonal elements $\overline{n}_{xx}$); the effect of intraband coherences (off-diagonal elements $\overline{n}_{\overline{x}x}$ with $\overline{x} \neq x$) will not be analyzed in this paper.

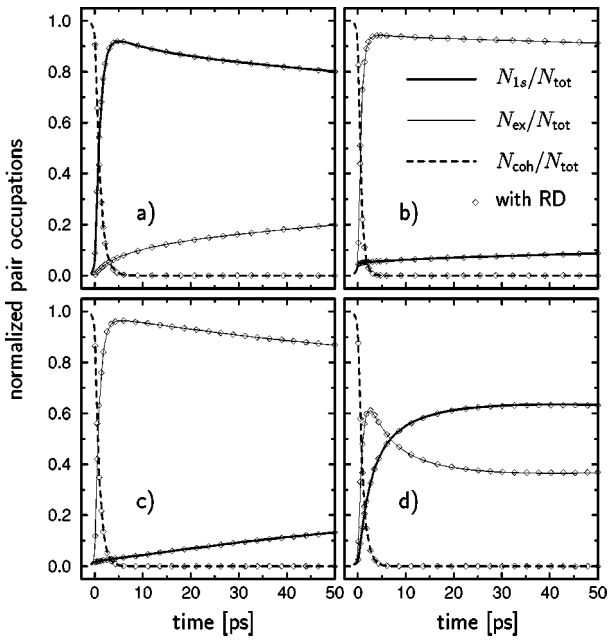

FIG. 4. Pair occupations normalized to N_{tot} for excitation energies relative to the band edge: (a) -18, (b) 0, (c) 10, (d) 20 meV. The curves are calculated without radiative decay. Diamonds are calculated including radiative decay.

Figure 4 shows the ratios of N_{coh} (dashed), N_{1s} (thick solid) and N_{ex} (thin solid) with respect to the total pair density N_{tot} for our four excitation scenarios. In this calculation all scattering mechanisms are included using a value of $\sigma_{IR} = 0.02$ meV/ps for the strength of the interface roughness. The curves correspond to calculations where the radiative decay has been neglected. We have also performed calculations including the radiative decay shown as diamonds in Fig. 4. As can be seen from the figure there is no noticeable effect on our results on the time scale studied here. We have therefore neglected the radiative decay in the rest of our studies.

At the pulse maximum (at time $t=0$ ps) the coherent density comprises almost the total pair density. The conversion from coherent excitations towards incoherent occupations starts already during the optical generation and is completed after a few picoseconds in all cases. The most remarkable finding is, however, that the relevant time scale for the formation of excitons changes by orders of magnitude depending on the excitation conditions. The individual results for our four scenarios are as follows.

For resonant excitation [Fig. 4(a)] about 90% of the pairs are in states on the 1*s* parabola at the end of the conversion process. The various scattering mechanisms lead to a partial dissociation of excitons into unbound electron-hole pairs such that after 50 ps the ocupation of the 1*s* parabola has dropped to 80% of N_{tot} while the remaining 20% occupy excited pair states.

The situation is very different when the central frequency coincides with the band edge [see Fig. 4(b)]. After the inital conversion of coherent excitations there are more than 90% of the pairs in excited states. Following the conversion only a very small increase of N_{1s} and a corresponding decrease of N_{ex} takes place on the time scale of 50 ps. This means that exciton formation is a very slow process for excitations at the band edge. Nevertheless, a population on the 1*s* parabola of about 5% of N_{tot} is built up already on a very short time scale and results from absorption of the low energy tail of the pulse spectrum at the 1*s* exciton (see Fig. 1). Thus, these pairs are generated from the start as excitons and are not formed from excited pairs in a scattering event.

A further increase of the excitation energy towards 10 meV above the band gap again alters the formation dynamics as can be seen from Fig. 4(c). Now there is only very little tail absorption at the 1*s* exciton and consequently almost all pairs are in excited states after the coherences have been converted into incoherent densities. However, the exciton formation has become noticeably faster than directly at the band edge such that after 50 ps an exciton population of more than 10% of the total density has built up, resulting mostly from exciton formation and not from tail absorption.

Finally, Fig. 4(d) displays results for an excitation above the threshold for LO phonon emission. Although crossing the LO threshold has only little effect on the decoherence (see Fig. 2), it has a dramatic impact on the exciton formation dynamics. LO phonon emission turns out to be a very efficient exciton formation process. Already in the time regime where coherent densities are still present a noticable occupation of exciton states has been built-up although tail absorption can be neglected under these excitation conditions. The maximum of the excited state population is limited by the rapid formation of excitons and never rises noticeably above 60% of N_{tot}. After about 7 ps the exciton population even surpasses the population of exited states and eventually saturates. After 50 ps more than 60% of the pairs occupy states on the 1*s* parabola.

At this point we would like to recall that for a given temperature there is a unique thermal pair distribution. In view of the fact that all calculations have been performed for the same temperature of $T=80$ K it is therefore interesting to note that there are obviously large differences in the distributions found after 50 ps for the four scenarios. Consequently, it has to be concluded that on this time scale the dynamics is still far from being relaxed to a thermal equilibrium. Calculations on a longer time scale up to times comparable with the radiative decay times indicate that the thermalization is not completed before the pair occupations start to decay in interband relaxation processes.[49]

C. Time-resolved exciton c.m. distribution

Following the time evolution of the total number N_{1s} of excitons on the 1*s* parabola gives a global estimate for the efficiency of exciton formation. However, most measurements are not sensitive to this quantity. Instead, typical observables usually scan only small portions of the 1*s* parabola. The best known example is the conventional excitonic luminescence which is determined by exciton densities in a small region near $K=0$. But, as mentioned earlier, there are more refined experimental techniques that are able to deliver a direct picture of the *K* distribution on the 1*s* parabola.[25,52–54] It is therefore important to know in which *K*

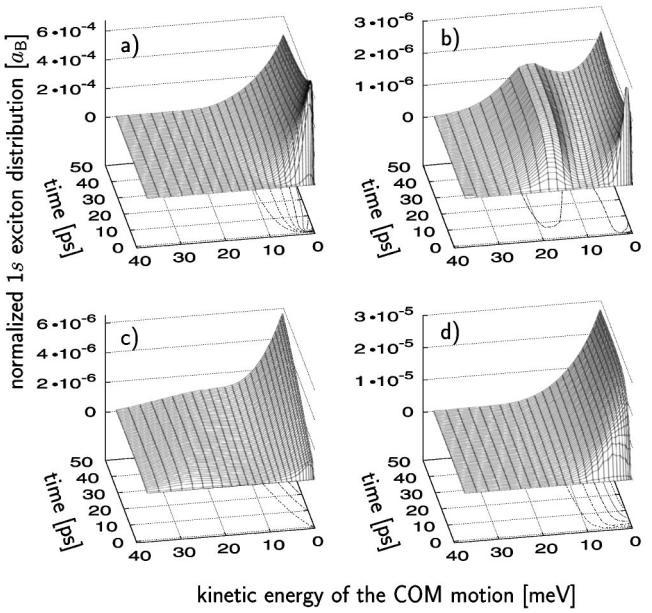

FIG. 5. Time evolution of the K-space distribution of incoherent $1s$ excitons normalized to N_{tot} in units of the bulk Bohr radius a_B for excitation energies relative to the band edge: (a) -18, (b) 0, (c) 10, (d) 20 meV.

regions the excitons are formed and how the resulting K distribution evolves in time. To this end we have analyzed in Fig. 5 the K-space distribution of incoherent $1s$ excitons normalized to N_{tot}. The normalization means that the K integral over this quantity equals N_{1s}/N_{tot}. As in the previous section we have accounted for all scattering mechanisms and the parts (a)–(d) of Fig. 5 refer to our four different excitation scenarios.

Even with a coarse view on Fig. 5 it becomes clear that the resulting K-space distributions on the $1s$ parabola dramatically change with changing excitation conditions. The different distributions reflect the competition between different physical processes and their changing relative importances. Each scattering mechanism is distinguished by a characteristic transfer of energy and momentum corresponding to specific pathways in the diagram of Fig. 1. Thus a noticeable contribution from one of the scattering mechanisms leads to a corresponding *fingerprint* in the resulting pair distribution. An analysis of the distributions for our four scenarios therefore yields a clear picture of the relevant physical processes for the respective excitation conditions. For our four cases we find the following individual results.

An excitation in resonance with the $1s$ exciton [part (a) of Fig. 5] generates an incoherent exciton population which is concentrated in a small K space region near $K=0$ for all times. A closer inspection of the figure reveals that within the first few picoseconds after the excitation the maximum is at a finite value of K and then moves towards $K=0$. This is the expected behavior because a conversion without momentum transfer is forbidden by energy and momentum conservation. Consequently, the conversion process necessarily generates in a first step incoherent exciton populations with a finite c.m. kinetic energy. A subsequent scattering event, which

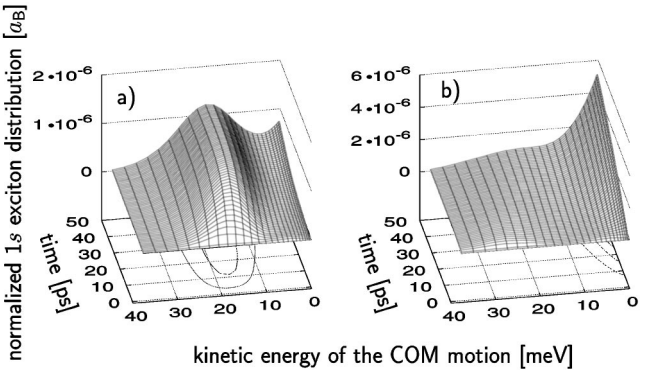

FIG. 6. Time evolution of the K-space distribution of incoherent $1s$ excitons normalized to N_{tot} in units of a_B neglecting y_{1s}, i.e., without $1s$ absorption, for excitation energies relative to the band edge: (a) 0, (b) 10 meV.

takes extra time, is needed to obtain an incoherent population at $K=0$. With increasing time the population near $K=0$ decreases and broadens due to redistributions on the $1s$ parabola (exciton heating).[17,26,27] and due to dissociation. The latter process was not discussed in previous studies.[17,26,27] It reduces the exciton population by about 20% within 50 ps, as already noted in Fig. 4(a).

Tuning the laser frequency to the band edge two distinct maxima show up in the exciton distribution [part (b) of Fig. 5]. A broad structure around kinetic energies close to the exciton binding energy and a narrow peak near $K=0$. The broad structure is due to formation processes where electron-hole pairs are scattered from the band edge almost horizontally in the scheme of Fig. 1 towards the $1s$ parabola. Such transitions can only result from scattering either with accoustic phonons or with interface roughness. While the broad structure in Fig. 5 takes of the order of 10 ps to rise the peak around $K=0$ is built-up almost instantaneously. This peak results from absorption of the low energy tails of the pulse spectrum directly at the $1s$ exciton and is therefore not connected to exciton formation. In order to separate the influences of tail absorption and exciton formation we have performed a calculation where the amplitude y_{1s} was set to zero by hand. As this amplitude is directly responsible for the absorption at the $1s$ exciton setting it to zero means that the $1s$ absorption has been switched off in this calculation. And indeed, without $1s$ absorption there is no peak near $K=0$ in the incoherent $1s$ K space distribution as can be seen from Fig. 6(a). Instead, a population with small K builds up slowly reflecting the relaxation of excitons formed initially with higher kinetic energies. It is interesting to note that for laser excitation at the band-gap the pulse spectrum of our 250 fs pulse has already droped significantly at the $1s$ resonance (see Fig. 1). But obvioulsy this effect is overcompensated by the large oscillator strength of the $1s$ exciton still leading to a considerable $1s$ population resulting from $1s$ absorption.

Figure 5(c) displays results for an increased excitation energy which is still below the LO threshold. The distribution exhibits two components. A contribution near $K=0$ and a rather flat and broad population initially centered at a kinetic energy corresponding to the energy difference between

the center of the excitation and the 1*s* exciton energy. Although the overlap of the pulse spectrum with the exciton line has further dropped the steep onset of the $K=0$ component is still due to tail absorption as demonstrated in Fig. 6(b) where the result of a corresponding calculation without 1*s* absortion is shown. The energetic position of the broad component suggests that for early times most pairs are scattered into states with energies close to the position of their optical generation. Again exciton formation proceeds mostly via horizontal transitions to the 1*s* parabola. With progressing time the center of the broad distribution shifts towards lower energies reflecting, on the one hand, the relaxation towards lower energies within the continuum before the exciton formation takes place and, on the other hand, the relaxation on the 1*s* parabola that follows the formation. The relaxation on the 1*s* parabola provides for a continuous flow towards states near $K=0$. However, the rise of the population near $K=0$ is significantly faster than in Fig. 5(b). Due to the scattering within the continuum a certain portion of pairs that have been generated below the LO threshold will now be lifted above the threshold. Thus LO phonon emission becomes a feasible process for these pairs leading to an increasing exciton formation rate. Excitons formed in this way must necessarily have c.m. momenta near $K=0$. It will be demonstrated below that LO phonon emission enabled by a broadening of the distribution due to acoustic phonon scattering is the main reason for the increased exciton formation efficiency found for this excitation condition.

When the excitation energy is further increased above the LO threshold, almost all of the excitons occupy states with small *K* values [see Fig. 5(d)]. A high energetic componentent at the position of the optical generation is not resolved compared with the bulk of the population near $K=0$. Obvioulsly, this distribution mainly reflects the high efficiency of the LO phonon emission process for the exciton formation. Energy conservation relevant for this process forces the excitons to be formed near $K=0$ because the excitation is located only slightly above the LO threshold. It is interesting to note that the initial width of the *K*-space distribution in Fig. 5(d) may be changed by changing the spectral width of the excitation as can be understood from the following argument. For excitation above the LO threshold, at early times excitons are formed due to LO emission by a conversion from coherent densities $|y_\nu|^2$ of continuum states. The *K* space position of the formed exciton is fixed by energy conservation and corresponds to an energy strictly $\hbar\omega_{\mathrm{LO}}$ below the energy of the initial state ν. Thus the width of the resulting *K* space distribution reflects the width of the portion of the pulse spectrum that lies above the LO threshold. In contrast, for resonant excitation [see Fig. 5(a)] the width is determined by a different mechanism which is essentially independent of the pulse spectrum. Here, only a single coherent amplitude, namely y_{1s}, has apreciable values. The corresponding coherent density $|y_{1s}|^2$ is converted mainly by deformation potential scattering with LA phonons [see Fig. 2(a)] and redistributed over the states on the 1*s* parabola. Consequently, the width of the resulting distribution is determined by the effective *K* space range of the deformation potential coupling which is limited primarily by the excitonic and the confinement form factors in Eq. (14). Thus in general different widths in *K* space have to be expected for excitation at the 1*s* exciton or above the LO threshold. For our specific parameters the latter turns out to be broader.

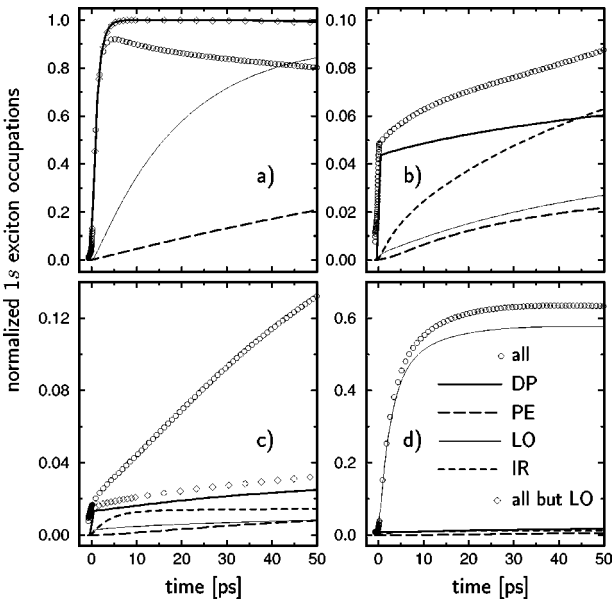

FIG. 7. Normalized 1*s* exciton density for different excitation energies relative to the band edge: (a) −18, (b) 0, (c) 10, (d) 20 meV. The curves account for different scattering mechanisms: circles: all mechanisms are included, DP: deformation potential scattering, PE: piezoelectric coupling, LO: Fröhlich coupling, IR: interface roughness scattering with $\sigma_{\mathrm{IR}}=0.02$ meV/ps, diamonds: all mechanisms except for Fröhlich coupling are included.

D. Impact of various interactions on the exciton formation dynamics

In order to analyze the relative importance of the various interactions we have performed calculations where exclusively a single mechanism has been included. The results are plotted in Fig. 7. Apart from the dramatic dependence of the exciton formation efficiency, which was already noted in Fig. 4, the most striking feature of Fig. 7 is that the exciton population obtained by accounting simultaneously for all mechanisms is typically very different from the sum of the contributions resulting from calculations for each individual mechanism. This nonadditivity indicates interesting combination effects between different scattering mechanisms which are characteristic for each of our four excitation scenarios.

For resonant excitation of the 1*s* exciton [Fig. 7(a)] all mechanisms would predict a monotonous rise of N_{1s}/N_{tot} when they were the only process present. Nevertheless, the combined action of these processes yields a nonmonotonous curve with a maximum at about 5 ps due to a fast initial rise produced by deformation potential scattering followed by a slower reduction of the exciton population as a consequence of dissociation processes which are induced by the absorption of LO phonons. This interpretation is confirmed by a calculation where LO phonon scattering has been selectively

switched off [diamonds in Fig. 7]. The resulting curve is almost indistinguishable from the calculation for deformation potential scattering alone, thus demonstrating that the reduction in the full calculation is indeed due to LO phonon absorption.

Figure 7(b) shows the results for excitation at the band edge. Here, N_{1s}/N_{tot} exhibits an almost steplike onset followed by a much flatter continuous rise at later times. The calculations for different mechanisms reveal that the steep onset is produced by deformation potential scattering with LA phonons. As discussed earlier under these excitation conditions direct excitonic absorption is still appreciable resulting in the peak structure near $K=0$ in Fig. 5(b). Therefore, we attribute the rapid initial rise to this process. Scattering by acoustic phonons either by deformation potential or piezoelectric coupling leads only to a small additional increase of the exciton population after this initial step. Interactions with acoustic phonons favor scattering events accompanied by small momentum transfers. However, exciton formation by acoustic phonon scattering necessarily requires a sizable transfer of momentum due to energy conservation in connection with the linear dependence of the phonon energy on the phonon momentum. Therefore, these mechanisms are rather inefficient in forming excitons although piezoelectric scattering dominates the decoherence at the band edge [see Fig. 2(b)]. We thus conclude that the exciton formation from unbound pairs at the band-edge is mainly due to interface roughness.

Figure 7(c) refers to a pulse energy just below the LO threshold. Even for this rather large spectral separation of the excitation from the $1s$ exciton line there is still a noticeable steplike onset in the contribution from the deformation coupling which is related to tail absorption [see Fig. 6(b)]. However, the most interesting aspect of the figure is the strong nonadditivity of the various contributions from individual scattering mechanisms. The exciton population obtained by accounting simultaneously for all mechanisms is much larger than the sum of the individual contributions. We attribute this effect to LO phonon emission enabled by the broadening of the distribution due to other processes. LO phonon emission alone gives a rather small contribution to the exciton population because most of the pairs are generated by the laser below the LO threshold. Exciton formation by one of the other processes is rather unlikely, too, because of the large energy and momentum transfer needed in order to reach the $1s$ parabola. But combining these processes results in a considerably increased formation of excitons by first lifting the pairs above the threshold and then emitting a LO phonon. In order to verify this interpretation we have plotted in Fig. 7(c) a curve where all mechanisms except for LO phonon scattering have been accounted for [diamonds in Fig. 7(c)]. This curve demonstrates that the dramatic increase of the formation efficiency found in the full calculation is indeed the result of the emission of LO phonons enabled by the broadening of the pair distribution due to acoustic phonon absorption.

Finally, plotted in Fig. 7(d) are the exciton occupations that build up after excitation above the LO threshold. As is clearly seen in the figure, LO phonon scattering dominates

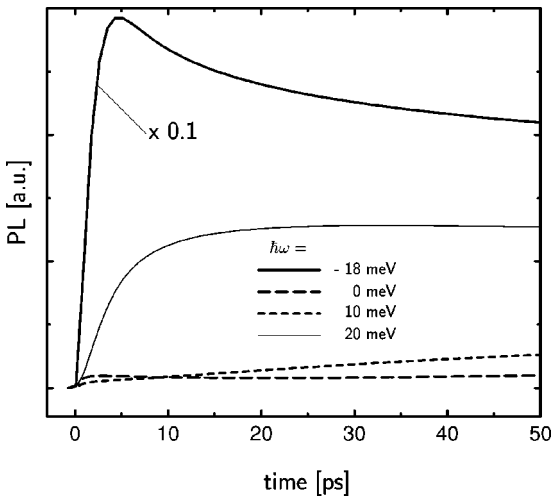

FIG. 8. Calculated photoluminescence signal emitted due to the radiative decay of $1s$ exciton states. The signal is integrated over all emission angles. The calculations correspond to different excitation energies $\hbar\omega$ relative to the band edge. The curve for resonant excitation at the $1s$ exciton at -18 meV has been scaled by a factor of 0.1.

by far the formation process over all other contributions. By fitting an exponential rise proportional to $[1-\exp(-t/\tau)]$ we have extracted a value of $\tau\approx 4$ ps which may be identified with an exciton formation time. Corresponding fits for excitations below the LO threshold [parts (b) and (c) of Fig. 7] yield values of the order of $\tau\approx 230$ ps [part (b)] and $\tau\approx 150$ ps [part (c)], respectively.[61] In these cases the functional form of the curves is not strictly exponential; nevertheless the extracted numbers reflect roughly the duration of the rises and confirm that the formation takes place on a much longer time scale than for excitations above the LO threshold which is also obvious from the figures.

E. Excitonic luminescence

It has been noted above that all K components of the $1s$ exciton distribution are in principle accessible in suitably designed experiments.[25,52–54] However, standard photoluminescence measurments are only sensitive to the densities near $K=0$. In order to make the connection between our theory and standard measurments more explicit we have determined the emitted excitonic photoluminescence intensity. To this end we have applied the theory presented in Ref. 27 and calculated the photon-assisted polarizations $\langle \hat{Y}(b_q^\dagger - \langle b_q^\dagger\rangle)\rangle$ ($b_q^\dagger$ are creation operators for photons with wave vector q) from which the luminescence signal can be derived immediately.[39,27] It has been verified in Ref. 27 that it is usually sufficient to determine the photon-assisted polarizations in Markov approximation. Therefore, we have also applied this approximation in our present calculation.

Figure 8 displays the resulting angle averaged excitonic photoluminescence signals for our four excitation scenarios. Our main prediction is that in the low excitation regime the rise time of the photoluminescence of a quantum wire should dramatically depend on the excitation frequency reflecting the changes in the exciton formation efficiency.

IV. CONCLUSIONS

We have presented a microscopic theory allowing for a consistent treatment of the combined dynamics of coherent and incoherent electron-hole pairs for excitations below and above the band-gap. We have applied our theory to a GaAs quantum-wire model. The relative importance of a great variety of scattering mechanisms relevant at low excitation densities has been analyzed for varying excitation conditions and in different dynamical regimes. The range of the investigated regimes covers the dynamics of coherently excited pairs as well as their conversion into incoherent occupations and eventually a regime of incoherent redistributions which includes the formation of incoherent populations on the 1*s* parabola. Our studies reveal that the decoherence in the vicinity of the band edge at a temperature of 80 K is dominated by acoustic phonon scattering. Compared with deformation potential scattering all other mechanisms are negligible for excitations in resonance with the 1*s* exciton. Above the band-gap piezoelectric coupling gives the fastest contribution to the conversion from coherent into incoherent pairs, but deformation potential scattering is also of comparable magnitude. Crossing the threshold for transitions towards the 1*s* parabola by LO phonon emission does not significantly accelerate the decoherence. Nevertheless, LO phonon emission turns out to be the most efficient process for forming excitons whenever it is energetically allowed. For excitations at the LO threshold we find an exciton formation time of the order of 4 ps. Tuning the laser frequency towards lower energies but still above the band gap the exciton formation process slows down significantly. This dramatic dependence on the excitation energy is also reflected in the corresponding photoluminescence signals.

The most important general insight implied by our present analysis is, however, that the dynamics of pairs in the vicinity of the semiconductor band edge is not dominated by a single scattering process. Instead, there is a competition of many processes of similar magnitudes. In particular, scattering by TA and LA phonons via different coupling mechanisms is as important as LO phonon scattering or interface roughness. The absolute values of the relative weights of the mechnanisms depend crucially on the excitation conditions. But it seems to be a general characteristic of a physical situation with many competing processes of comparable magnitudes that the combined effect of all contributions is quantitatively and in some cases even qualitatively different from the sum of the effects provoked by each of the mechanisms individually.

ACKNOWLEDGMENTS

This work was supported by the Deutsche Forschungsgemeinschaft through the program *Quantenkohärenz in Halbleitern* and a *Habilitationsstipendium* for V.M.A. as well as by the Eurorean Union through the TMR network *Ultrafast Quantum Optoelectronics*.

APPENDIX: ON THE CHOICE OF THE BASIS

In principle, any quantum mechanical problem may be formulated in any basis without affecting predictions for observables. But whenever use is made of a Markov approximation the result will in general depend on the basis because by specifying the initial and the final states of a possible scattering process one determines the relevant quasiparticles of the system. In particular, the Markov approximation enforces a strict conservation of quasiparticle energies for each scattering event. Thus, as a consequence of performing the Markov approximation in the pair basis the arguments of the energy conserving delta functions in all our scattering matrices connect pair energies [see Eqs. (13),(19),(27)]. In contrast, *k*-space versions of the Markov approximation enforce the energy conservation with respect to single particle energies.[32,39,62] These different formulations of the energy conservation indeed lead to significantly different predictions as may be seen by comparing the energetics of the emission of a LO phonon in both approaches. By considering energy conservation in the pair basis the LO phonon emission becomes possible for pair energies higher than one LO phonon energy above the energy of the 1*s* exciton. The corresponding threshold enforced by the conservation of single particle energies is found at pair energies which are at least one LO phonon energy above the band edge. In view of this basis dependence care should be taken to find a basis that is particularly adapted to the situation studied. In order to address clearly the aspects most relevant for the choice of the basis in our case, we will discuss briefly the physical implications for the formation of excitons that result from the steps involved in the Markov approximation. To this end we take the interaction with LO phonons as an example and start our analysis from a quantum kinetic formulation of the dynamics in *k* space before the Markov approximation has been performed. For simplicity we will concentrate here on the coherent transition amplitudes, similar considerations apply to the incoherent densities. Within a quantum kinetic description the interaction with LO phonons provides for a source term[17,32]

$$Q_Y^{\mathrm{LO}} \equiv \sum_q \left[Y^{(-)}_{k+q,k} - Y^{(+)}_{k-q,k} - Y^{(-)}_{k,k-q} + Y^{(+)}_{k,k+q} \right] \quad \text{(A1)}$$

in the equation of motion for the interband transition density $Y_k \equiv \langle d_{-k} c_k \rangle$ in *k*-space representation. This source makes the coupling to the phonon assisted transition density matrices

$$Y^{(+)}_{k,k+q} := \frac{i}{\hbar} \gamma_{\mathrm{LO},q} \langle d_{-k} c_{k+q} b_q^\dagger \rangle, \quad \text{(A2)}$$

$$Y^{(-)}_{k+q,k} := \frac{i}{\hbar} \gamma_{\mathrm{LO},q} \langle d_{-(k+q)} c_k b_q \rangle \quad \text{(A3)}$$

explicit (b_q and $b_q^\dagger$ are Boson operators for a LO phonon with momentum q). For low excitation densities the equation of motion for $Y^{(\pm)}$ reads[17]

$$\partial_t Y^{(\pm)}_{k',k} = \frac{1}{i\hbar} \left[\left(\varepsilon^{\mathrm{e}}_k + \varepsilon^{\mathrm{h}}_{-k'} \mp \hbar \omega_{\mathrm{LO}} \right) Y^{(\pm)}_{k',k} + \tilde{Y}^{(\pm)}_{k',k} \right] \mp \frac{|\gamma_{\mathrm{LO},k'-k}|^2}{\hbar^2} \left(n_{\mathrm{LO}} + \frac{1}{2} \mp \frac{1}{2} \right) (Y_{k'} - Y_k). \quad \text{(A4)}$$

Here, n_{LO} is the thermal LO phonon occupation number, $\varepsilon_k^{e/h}$ are single particle energies for electrons and holes and $\tilde{Y}^{(\pm)}_{k',k}$ is defined as

$$\tilde{Y}^{(\pm)}_{k',k} := -\sum_q V_q Y^{(\pm)}_{k'+q,k+q}, \tag{A5}$$

where V_q is the Coulomb potential. It is important to note that although quantum kinetics is approximate, because use has been made of the correlation expansion, the truncation procedure does not introduce a basis dependence of the results, in contrast to the Markov approximation. Performing the Markov approximation involves two steps: (i) one has to formally invert the Eq. (A4) and insert the result in Eq. (A1) leading to a memory kernel that couples the transition amplitudes Y to their values at all earlier times, (ii) the essential time dependence of Y has to be determined up to a slowly varying factor which is then taken out of the memory integral. The evaluation of the remaining integral finally yields the energy conserving delta functions.

The second step determines the initial states of the scattering. In k-space representation it is usually assumed that the functions $\overline{Y}_k := \exp[i(\varepsilon_k^{\mathrm{e}} + \varepsilon_{-k'}^{\mathrm{h}})t/\hbar] Y_k$ are slowly varying thus implying that before the scattering the pairs are essentially made-up of free particles. As a result of identifying the factor $\exp[i(\varepsilon_k^e + \varepsilon_{-k'}^h)t/\hbar]$ with the essential time dependence the energies $\varepsilon_k^e + \varepsilon_{-k'}^h$ show up as arguments of the energy conserving delta functions after the evaluation of the time integral over the memory kernel. In contrast, when the Markov approximation is performed in the pair representation one identifies $\overline{y}_x := \exp(i\omega_x t) y_x$ with the slowly varying part of y_x. Here, the factor $\exp(i\omega_x t)$ is responsible for finding $\hbar\omega_x$, i.e., the energies of correlated pairs, as energies of the initial states in the delta functions, thus accounting for Coulomb induced correlations of the pairs before the scattering takes place. It should be noted that the possibility that electron-hole pairs may in fact be uncorrelated is also included as a limiting case in the treatment in the pair basis. In this case $\hbar\omega_x$ simply reduces to $\varepsilon_k^{\mathrm{e}} + \varepsilon_{-k'}^{\mathrm{h}}$. But the reverse is, of course, not possible, because there is no way to obtain correlated pair energies as a limiting case of free particle energies.

The final states of the scattering are the eigenstates of the homogeneous part of Eqs. (A4).[63] But, in order to obtain a numerically feasible procedure it is common practice to keep only those contributions to the homogeneous parts of the Eq. (A4) that are diagonal in the basis used. In the k-space basis this amounts to dropping the Coulomb induced terms $\tilde{Y}^{(\pm)}_{k',k}$ thus fixing also the final states to be plane waves. However, these Coulomb terms are of high importance for the physics of exciton formation or dissociation. They account for the fact that when a phonon hits a carrier that is tied within a pair it is not possible that the phonon energy is completely converted into kinetic energy of the carrier. Instead, a certain amount of energy is needed to work against the Coulomb forces represented by the potential in Eq. (A5). For near band-gap excitation this effect makes a great difference for all scattering processes discussed in this paper, especially for those interactions that typically transfer an energy that is small compared with the exciton binding energy. In contrast to the k-space version, the Markov approximation performed in the pair basis accounts for these Coulomb terms, because in pair representation the complete homogeneous part of Eq. (A4) including $\tilde{Y}^{(\pm)}_{k',k}$ is diagonal. Thus $\tilde{Y}^{(\pm)}_{k',k}$ is taken into account when the formal inversion is performed in the pair basis and the energies occuring in the delta functions of both the initial and the final states are the energies of correlated pairs. These considerations strongly suggest that the pair representation is the basis of choice when exciton formation is studied in Markov approximation.

A further advantage of the pair representation in this context is that there is a clear distinction between carriers bound within an exciton and carriers in scattering states. In some sense the electron and hole densities occuring in phenomenological three particle models can be identified within our approach with the corresponding particles in scattering states without introducing any overlap with particles bound in excitons. However, this does not imply a microscopical justification of these models, because from the electron and hole densities alone it is not possible to reconstruct the pair densities needed to account for Coulomb correlations during the scattering process. Therefore, a closed set of equations based on the densities of electrons, holes, and excitons is not obtainable from our microscopic equations without neglecting Coulomb correlations.

[1] J. Feldmann, G. Peter, E.O. Göbel, P. Dawson, K. Moore, C. Foxon, and R.J. Elliot, Phys. Rev. Lett. **59**, 2337 (1987).
[2] J. Kusano, Y. Segawa, Y. Aoyagi, S. Namba, and H. Okamoto, Phys. Rev. B **40**, 1685 (1989).
[3] T.C. Damen, J. Shah, D.Y. Oberli, D.S. Chemla, J.E. Cunningham, and J.M. Kuo, Phys. Rev. B **42**, 7434 (1990).
[4] R. Strobel, R. Eccleston, J. Kuhl, and K. Köhler, Phys. Rev. B **43**, 12 564 (1991).
[5] P. Roussignol, C. Delalande, A. Vinattieri, L. Carraresi, and M. Colocci, Phys. Rev. B **45**, 6965 (1992).
[6] P.W.M. Blom, P.J.v. Hall, C. Smit, J.P. Cuypers, and J.H. Wolter, Phys. Rev. Lett. **71**, 3878 (1993).
[7] A. Vinattieri, J. Shah, T.C. Damen, D.S. Kim, L.N. Pfeiffer, M.Z. Maialle, and L.M. Sham, Phys. Rev. B **50**, 10 868 (1994).
[8] T. Amand, B. Dareys, B. Baulac, X. Marie, J. Barrau, M. Brousseau, D.J. Dunstan, and R. Planel, Phys. Rev. B **50**, 11 624 (1994).
[9] D. Robart, X. Marie, B. Baylac, T. Amand, M. Brouseau, G. Bacquet, G. Debart, R. Planel, and J.M. Gerard, Solid State Commun. **95**, 287 (1995).
[10] R. Kumar, A.S. Vengurlekar, S.S. Prabhu, J. Shah, and L.N. Pfeiffer, Phys. Rev. B **54**, 4891 (1996).

[11] S. Grosse, R. Arnold, G.v. Plessen, M. Koch, J. Feldmann, V.M. Axt, T. Kuhn, R. Rettig, and W. Stolz, Phys. Status Solidi B **204**, 147 (1997).
[12] X. Marie, J. Barrau, P.L. Jeune, T. Amand, and M. Brousseau, Phys. Status Solidi A **164**, 359 (1997).
[13] R. Kumar, A.S. Vengurlekar, A. Gopal, T. Mélin, F. Laruelle, B. Etienne, and J. Shah, Phys. Rev. Lett. **81**, 2578 (1998).
[14] M. Gurioli, P. Borri, M. Colocci, M. Gulia, F. Rossi, E. Molinari, P.E. Selbmann, and P. Lugli, Phys. Rev. B **58**, 13 403 (1998).
[15] P. Borri, W. Langbein, J.M. Hvam, and F. Martelli, Phys. Rev. B **59**, 2215 (1999).
[16] P.E. Selbmann, M. Gulia, F. Rossi, E. Molinari, and P. Luigli, Phys. Rev. B **54**, 4660 (1996).
[17] V.M. Axt, K. Siantidis, M. Herbst, T. Kuhn, S. Grosse, M. Koch, and J. Feldmann, Mater. Sci. Forum **297-298**, 79 (1999).
[18] C. Piermarocchi, F. Tassone, V. Savona, A. Quattropani, and P. Schwendimann, Phys. Rev. B **55**, 1333 (1997).
[19] C. Piermarocchi, V. Savona, A. Quattropani, P. Schwendimann, and F. Tassone, Phys. Status Solidi A **164**, 221 (1997).
[20] C. Piermarocchi, V. Savona, A. Quattropani, P. Schwendimann, and F. Tassone, Phys. Status Solidi B **204**, 191 (1997).
[21] M.H. Zhang, Q. Huang, and J.M. Zhou, J. Phys.: Condens. Matter **9**, 10 185 (1997).
[22] M. Gulia, F. Rossi, E. Molinari, P.E. Selbmann, F. Compagnone, and P. Lugli, Phys. Status Solidi B **204**, 233 (1997).
[23] M. Gulia, F. Rossi, E. Molinari, P.E. Selbmann, and P. Lugli, Phys. Rev. B **55**, 16 049 (1997).
[24] I.-K. Oh, J. Singh, A. Thilagam, and A.S. Vengurlekar, Phys. Rev. B **62**, 2045 (2000).
[25] M. Umlauf, J. Hoffmann, H. Kalt, W. Langbein, J.M. Hvam, M. Scholl, J. Söllner, M. Heuken, B. Jobst, and D. Hommel, Phys. Rev. B **57**, 1390 (1998).
[26] V.M. Axt, T. Kuhn, K. Siantidis, S. Grosse, M. Koch, J. Feldmann, and W. Stolz, Proc. SPIE **3624**, 68 (1999).
[27] A. Thränhardt, S. Kuckenburg, A. Knorr, T. Meier, and S.W. Koch, Phys. Rev. B **62**, 2706 (2000).
[28] V.M. Axt and A. Stahl, Z. Phys. B **93**, 195 (1994); **93**, 205 (1994).
[29] A. Stahl and I. Balslev, *Electrodynamics of the Semiconductor Band Edge*, Vol. 110 of *Springer Tracts in Modern Physics* (Springer-Verlag, Heidelberg, 1987).
[30] H. Haug and S. W. Koch, *Quantum Theory of the Optical and Electronic Properties of Semiconductors*, 3rd ed. (World Scientific, Singapore, 1994).
[31] T. Takagahara, Phys. Rev. B **31**, 6552 (1985).
[32] T. Kuhn, in *Density Matrix Theory of Coherent Ultrafast Dynamics*, Vol. 4 of *Electronic Materials*, edited by E. Schöll (Chapman & Hall, London, 1998), Chap. 6.
[33] G. D. Mahan, *Many-Particle Physics*, 2nd ed. (Plenum Press, New York, 1990).
[34] T. Ando, A.B. Fowler, and F. Stern, Rev. Mod. Phys. **54**, 437 (1982).
[35] R. Zimmermann, Nuovo Cimento D **17**, 1801 (1995).
[36] A. Thänhardt, S. Kuckenburg, A. Knorr, P. Thomas, and S.W. Koch, Phys. Rev. B **62**, 16 802 (2000).
[37] D.S. Citrin, Phys. Rev. Lett. **69**, 3393 (1992).
[38] D.S. Citrin, Phys. Rev. B **47**, 3832 (1993).
[39] T. Kuhn and F. Rossi, Phys. Rev. B **46**, 7496 (1992).
[40] M. Kira, F. Jahnke, W. Hoyer, and S.W. Koch, Prog. Quantum Electron. **23**, 189 (1999).
[41] V.M. Axt and S. Mukamel, Rev. Mod. Phys. **70**, 145 (1998).
[42] M. Bonitz, J.W. Dufty, and C.S. Kim, Phys. Status Solidi B **206**, 181 (1998).
[43] W. Schäfer, R. Lövenich, N.A. Fromer, and D.S. Chemla, Phys. Rev. Lett. **86**, 344 (2001).
[44] T. Meier and S.W. Koch, Phys. Rev. B **59**, 13 202 (1999).
[45] R. Zimmermann, Phys. Status Solidi B **159**, 317 (1990).
[46] J. Schilp, T. Kuhn, and G. Mahler, Phys. Rev. B **50**, 5435 (1994).
[47] V.M. Axt, K. Viktor, and A. Stahl, Phys. Rev. B **53**, 7244 (1996).
[48] S. Savasta and R. Girlanda, Phys. Rev. B **59**, 15 409 (1999).
[49] K. Siantidis, T. Wolterink, V. M. Axt, and T. Kuhn, Physica B **314**, issue 1-4 March 2002 (to be published).
[50] V.M. Axt, G. Bartels, and A. Stahl, Phys. Rev. Lett. **76**, 2543 (1996).
[51] P. Haring Bolivar, F. Wolter, A. Müller, H.G. Roskos, H. Kurz, and K. Kohler, Phys. Rev. Lett. **78**, 2232 (1997).
[52] D.W. Snoke, D. Brown, and M. Cardona, Phys. Rev. B **44**, 2991 (1991).
[53] J. Shah, *Ultrafast Spectroscopy of Semiconductors and Semiconductor Nanostructures*, Vol. 115 of *Solid-State Science* (Springer-Verlag, Berlin, 1996).
[54] J. Hoffmann, M. Umlauff, H. Kalt, W. Langbein, and J. Hvam, Phys. Status Solidi B **204**, 195 (1997).
[55] G. D. Mahan, in *Polarons in Heavily Doped Semiconductors*, *Polarons in Ionic Crystals and Polar Semiconductors*, edited by J. T. Devreese (North-Holland, Amsterdam, 1972), Chap. VI, p. 533.
[56] R. Zimmermann, Phys. Status Solidi B **173**, 129 (1992).
[57] R. Zimmermann and E. Runge, J. Lumin. **60&61**, 320 (1994).
[58] The elastic contribution to the pair density in Eq. (24) has been shown to give rise to a distinct part of the secondary emission which has been called the *coherent* part in Ref. 36.
[59] K. Siantidis, V. M. Axt, J. Wühr, and T. Kuhn, Phys. Status Solidi B (to be published).
[60] For polar interactions the relation $\gamma_\mu^e = \gamma_\mu^h$ holds in Eq. (14) and thus this factor can be taken out of the integral. Due to the overall charge neutrality there are large compensations in the integrand of Eq. (14) especially when the wavefunctions involved are smooth extended functions in k space. The latter condition applies in particular for the spatially localized wavefunction of the $1s$ exciton but not for delocalized states in the electron-hole continuum.
[61] The fits were made to data with completed rises (not shown fully in the figures).
[62] A. Knorr, F. Steininger, B. Hanewinkel, S. Kuckenburg, P. Thomas, and S.W. Koch, Phys. Status Solidi B **206**, 139 (1998).
[63] This is seen most clearly when the Green-function needed to invert Eq. (A4) is expanded in the eigenbasis of the homogeneous problem, because then it becomes obvious that the energies of the final states occuring eventually in the arguments of the delta functions are the corresponding eigenenergies.
[64] Landolt and Börnstein, *Semiconductors: Physics of Group IV Elements and III-V Compounds* (Springer-Verlag, Berlin,Heidelberg, 1982).